NANO LETTERS

Letter

pubs.acs.org/NanoLett

Interface Formation in Monolayer Graphene-Boron Nitride Heterostructures

P. Sutter,* R. Cortes, J. Lahiri, and E. Sutter

Center for Functional Nanomaterials, Brookhaven National Laboratory, Upton, New York 11973, United States

Supporting Information

ABSTRACT: The ability to control the formation of interfaces between different materials has become one of the foundations of modern materials science. With the advent of two-dimensional (2D) crystals, low-dimensional equivalents of conventional interfaces can be envisioned: line boundaries separating different materials integrated in a single 2D sheet. Graphene and hexagonal boron nitride offer an attractive system from which to build such 2D heterostructures. They are isostructural, nearly lattice-matched, and isoelectronic, yet their different band structures promise interesting functional properties arising from their integration. Here, we use a combination of in situ microscopy techniques to study the growth and interface formation of monolayer graphene-boron nitride heterostructures on ruthenium. In a sequential chemical vapor deposition process, boron nitride grows preferentially at the edges of existing monolayer graphene domains, which can be exploited for synthesizing continuous 2D membranes of graphene embedded in boron nitride. High-temperature growth leads to intermixing near the interface, similar to interfacial alloying in conventional heterostructures. Using real-time microscopy, we identify processes that eliminate this intermixing and thus pave the way to graphene-boron nitride heterostructures with atomically sharp interfaces.

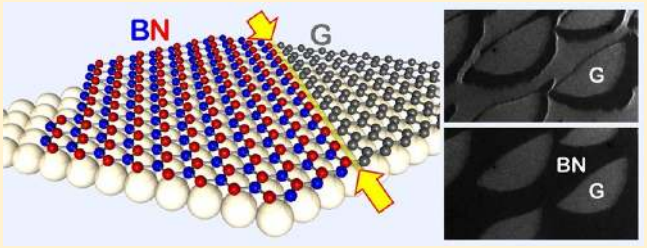

KEYWORDS: *Graphene, boron nitride, heterostructure, interface, chemical vapor deposition, microscopy*

First-principles calculations have predicted unusual electronic properties associated with the interfaces between monolayer graphene and boron nitride, such as the opening of a variable bandgap,[1−3] magnetism,[4] unique thermal transport properties,[5] robust half-metallic behavior[6] without applied electric fields,[7] and interfacial electronic reconstructions[8] analogous to those observed in oxide heterostructures.[9,10] Access to these properties depends on methods for controlling the formation of graphene-boron nitride interfaces within a single atomic layer. Techniques for the synthesis of two-dimensional (2D) materials on metal substrates have become increasingly well developed,[11−17] and variants of these methods may lend themselves to the growth of more complex heterostructures. Recent work on chemical vapor deposition (CVD) on Cu substrates has demonstrated the ability to generate graphene-boron nitride stacks[18] as well as domain-hybridized layers[19] by sequential and simultaneous exposure to C and B/N precursors, respectively. Intermixing, which can cause nonabrupt, graded boundaries, is a key issue of interface formation in conventional heterostructures as well as their monolayer analogs. Calculations have suggested that the conjugation and aromaticity within all-carbon segments should drive graphene and boron nitride to phase separate in free-standing membranes.[20] Few-layer hybrids on Cu provide evidence for separate graphene and boron nitride domains on the nanoscale[19] but do not address interface formation or offer insight into possible modifications of the phase behavior by a metal substrate. B and N doping of graphene have been demonstrated,[21,22] suggesting that atomic substitution is generally possible and could play an important role in the formation of 2D graphene-boron nitride heterostructures.

Figure 1 shows low-energy electron microscopy (LEEM) images of sequential graphene and boron nitride growth on Ru. Monolayer graphene (MLG) domains with characteristic lens shape, determined by differences in the graphene growth rate in relation to the direction of surface steps on Ru(0001),[12] are formed by exposing the substrate to ethylene. At partial graphene coverage, the ethylene supply is stopped, and the sample is subsequently exposed to borazine to initiate hexagonal boron nitride (h-BN) growth.[16] MLG and h-BN are easily distinguished by their different LEEM image contrast. At low BN coverage (Figure 1a), all h-BN attaches to edges of existing MLG domains; no nucleation of h-BN on the Ru surface away from MLG is observed. Longer borazine exposure leads to progressively larger BN coverage (Figures 1b,c). The h-BN expands anisotropically, similar to the growth of MLG/Ru(0001), with high rate along substrate terraces and downhill across steps and a lower rate in the uphill direction. Ultimately, the substrate is covered by a continuous layer comprising graphene domains embedded in boron nitride (Figure 1d). Our observations are consistent with large (several micrometers)

Received: June 27, 2012
Published: August 7, 2012

ACS Publications © 2012 American Chemical Society

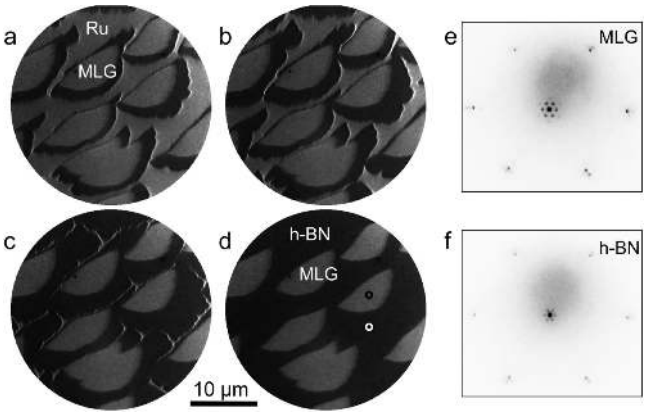

Figure 1. Real-time microscopy of the synthesis of monolayer graphene-boron nitride heterostructures. Borazine CVD growth of boron nitride (h-BN) by attachment to monolayer graphene (MLG) domains, formed by exposure of the Ru substrate to ethylene (10^{-8} Torr; 800 °C). Elapsed time: (a) 250 s; (b) 400 s; (c) 550 s; (d) 670 s. Temperature: 780 °C. Borazine pressure: 2×10^{-8} Torr (a,b); 6×10^{-8} Torr (c,d). (e) Microdiffraction pattern of MLG (2 μm aperture, centered on black circle in panel d). (f) Microdiffraction pattern of h-BN (centered on white circle in panel d).

diffusion lengths of the mobile N- and B-containing surface species, along with sufficiently low barriers allowing their preferential incorporation into the graphene edges and avoiding h-BN nucleation on the free Ru surface. Overall, the mesoscale growth characteristics suggest bonding of the graphene and boron nitride lattices at the atomic scale, which is confirmed below by scanning tunneling microscopy (STM).

The formation of a monolayer heterostructure of graphene domains surrounded by h-BN is corroborated by micro-LEED (Figure 1e,f). The graphene has the characteristic moiré structure of MLG/Ru(0001) with a coincidence lattice of approximately 12 × 12 [G] on 11 × 11 [Ru] unit cells (period ~29.8 Å, Figure 1e).[12,23] Similarly, the surrounding h-BN shows a uniform diffraction pattern consistent with a moiré structure of 13 × 13 [BN] on 12 × 12 [Ru] (period ~32.5 Å, Figure 1f).[16,24] Both the graphene and boron nitride lattices are aligned in-plane with the Ru(0001) surface mesh and are hence closely aligned relative to one another.

For epitaxial metal and semiconductor heterostructures, the higher dimensional equivalent of the supported heteromembranes produced here, atomically abrupt interfaces can be difficult to achieve[25,26] with stable interfacial mixtures forming even between bulk-immiscible elements.[27] We have used chemical analysis by ultrahigh-vacuum (UHV) nano-Auger electron spectroscopy (AES) to probe a possible intermixing in graphene-boron nitride heterostructures. AES confirms pure MLG and h-BN far from the interfaces (Figure 2a,b). In particular, only C is detected within MLG domains, which implies that borazine exposure of MLG/Ru does cause significant B or N incorporation into the graphene. This is consistent with a low reactivity of supported MLG, similar to h-BN/Ru,[16] suppressing borazine dissociation and substitution of B/N for C. Close to the MLG/h-BN interfaces, AES line scans indicate the formation of a mixed phase containing B, N, as well as C (Figure 2 c). The composition profile from the MLG domains into the surrounding h-BN is asymmetric. Accounting for the convolution with a finite-sized probe volume, it suggests an abrupt boundary in the slow growth direction and a broader tail with mixed composition in the direction of fast h-BN

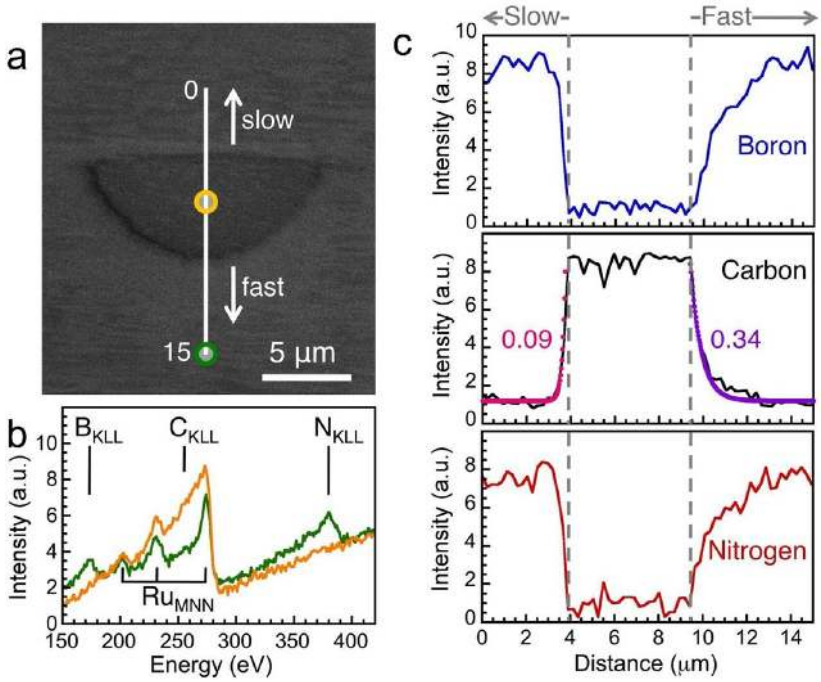

Figure 2. Nano-Auger spectroscopy analysis of a monolayer graphene-boron nitride heterostructure grown by sequential CVD at high temperature (800 °C). (a) UHV SEM image of a MLG domain embedded in a continuous h-BN layer. Arrows designate the fast (step down) and slow (step up) growth directions of both MLG and h-BN. (b) Auger electron spectra at points near the center of the MLG domain and in the h-BN layer, marked in (a). (c) Nano-AES line scans for B_{KLL} (171.6 eV), C_{KLL} (260.6 eV), and N_{KLL} (380.0 eV) Auger lines, along the line marked in (a). Points in the C_{KLL} line scan, representing exponential decay fits to the data, show the asymmetry in the near-interface composition profiles with half widths of 0.09 and 0.34 μm along the slow and fast h-BN growth directions, respectively.

dx.doi.org/10.1021/nl302398m | *Nano Lett.* 2012, 12, 4869−4874

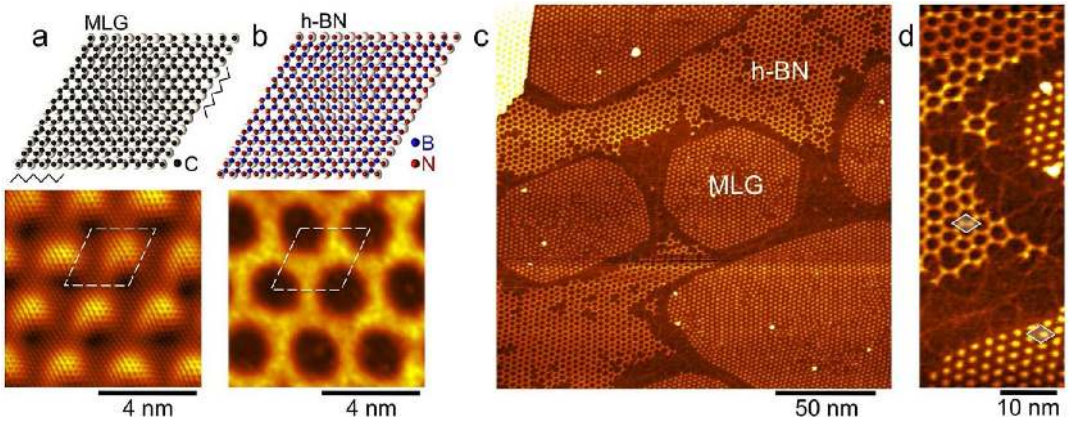

Figure 3. UHV STM of separate graphene, monolayer hexagonal boron nitride, and of graphene-boron nitride heterostructures on Ru(0001). (a) Ball and stick model showing the C and surface Ru layer (top) and STM image (bottom) of the monolayer graphene/Ru(0001) moiré structure. (b) Model (top) and STM image (bottom) of the h-BN/Ru(0001) moiré structure. For both graphene and h-BN, zigzag edges are aligned with the boundaries of the moiré unit cell. (c) Graphene-boron nitride heterostructure on Ru(0001). In addition to the pure (MLG; h-BN) phases, transition regions without the characteristic moiré structure exist near the interfaces. (d) High-magnification image of the graphene-boron nitride boundary.

growth. These findings are consistent with an intermixing mechanism involving primarily the incorporation of C into the growing BN. This C doping progressively diminishes as the surface C supply becomes depleted.

Excluding substitutional B/N doping of graphene, against which there is evidence from AES and atomic-resolution STM, the intermixing may either be due to (i) a direct exchange of MLG edge C atoms with B or N during borazine exposure; or (ii) incorporation of C from the Ru surface into the growing h-BN film. Direct exchange, which should be limited to the immediate vicinity of the interface where there is a high probability of C−B/N swaps, cannot explain the wide intermixed zones we observe. Hence, C incorporation into the growing h-BN lattice is likely the primary intermixing mechanism. For metal substrates such as Ru, the C can be supplied by two possible reservoirs: interstitial C,[12] or thermal C adatoms in equilibrium with graphene.[28] Experiments on bulk crystals and epitaxial Ru(0001) films with negligible C solubility[29] show identical results, suggesting C adatoms on the metal surface as the predominant C source.

We used UHV STM to determine the atomic-scale structure of the near-interface zone (Figure 3), which could either comprise phase-separated nanoscale graphene and boron nitride domains or a substitutional B−N−C "alloy" phase. The interpretation of the STM images is facilitated by characteristic moiré structures of MLG and h-BN on Ru(0001) with distinctly different appearance. The MLG/Ru moiré (Figure 3a) consists of a "high" or atop region, centered in one-half of the unit cell rhombus, where the C atoms occupy fcc and hcp hollow sites relative to surface Ru atoms, and two distinct "low" areas with (top, hcp) and (top, fcc) registry, respectively.[30,31] The h-BN/Ru moiré structure (Figure 3b) is made up of majority low regions with (fcc, top) registry, in which N and B atoms are close to the metal, surrounded by narrow, less strongly coupled high areas with registries close to (hcp, fcc) and (top, hcp).[32] Figure 3c shows a heterostructure, in which initial nanoscale graphene domains were prepared by room temperature ethylene adsorption on epitaxial Ru(0001), followed by dehydrogenation at 800 °C. Boron nitride was synthesized by subsequent exposure to borazine (10^{-7} Torr) at reduced temperature (750 °C). Coexisting MLG and h-BN areas are clearly visible. Their moiré structures are closely aligned in-plane (Figure 3d), consistent with micro-LEED. However, the moirés of the two materials never come atomically close but are invariably separated by an interfacial band (here up to ∼20 nm wide) that shows neither of the structures of pure MLG or h-BN on Ru.

High-resolution cryogenic STM images of the interfacial region (Figure 4) confirm that this zone has mostly h-BN like

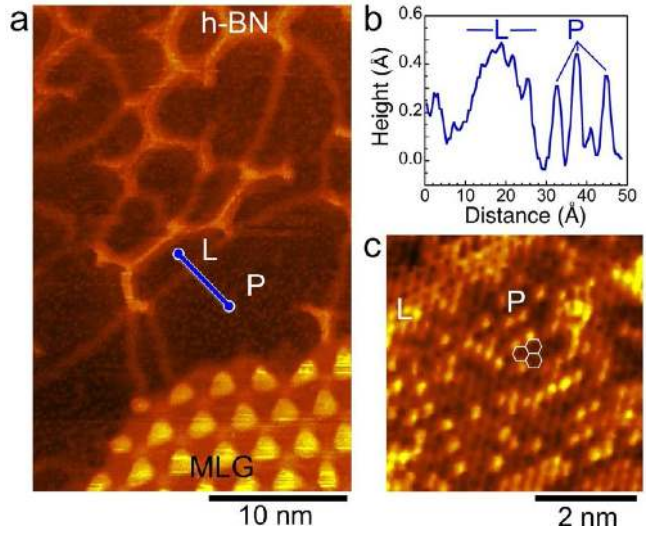

Figure 4. High-resolution cryogenic STM near the graphene-boron nitride interface. (a) Overview image, showing h-BN and MLG areas, separated by a flat interfacial zone with faint lines (L) and atomic-scale point-like protrusions (P). (b) Height profile along the line segment shown in (a). (c) High-magnification image of the flat near-interface zone, showing a honeycomb structure matching the h-BN atomic lattice and point-like protrusions. (Imaging parameters: V_S = +2.0 V; I = 1.0 nA).

character with apparent height close to the h-BN low regions and embedded higher moiré fragments. The graphene moiré structure terminates in an atomically sharp edge but a well-developed h-BN moiré appears only several nanometers away from this boundary. A network of shallow lines (L) and embedded point-like protrusions (P) are imaged with apparent heights of about 0.4 Å (Figure 4a,b). The protrusions coexist

dx.doi.org/10.1021/nl302398m | *Nano Lett.* 2012, 12, 4869−4874

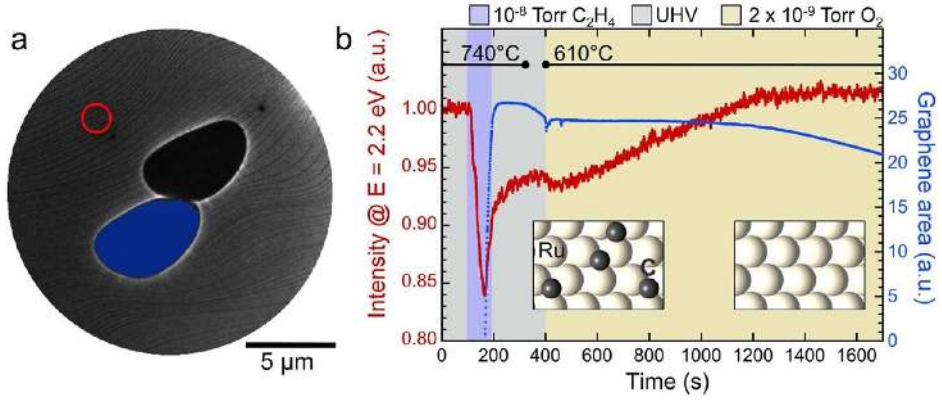

Figure 5. Controlled removal of C monomers from Ru(0001) near monolayer graphene domains. (a) LEEM image of a section of Ru(0001) surface adjacent to two monolayer graphene domains. (b) Simultaneous measurement of the LEEM $I-V$ intensity at $V = 2.2$ eV on Ru(0001) (within the red circle in panel a) and of the area of one graphene domain (shaded blue in panel a). Lower intensity corresponds to higher C adatom concentration. Graphene growth (10^{-8} Torr C_2H_4; 740 °C) is followed by O_2 exposure (2×10^{-9} Torr; 610 °C). A progressive increase in intensity accompanies the removal of C adatoms until saturation is reached at the level of clean Ru(0001). The area of the graphene domains remains nearly constant until the C adatoms are removed from the metal.

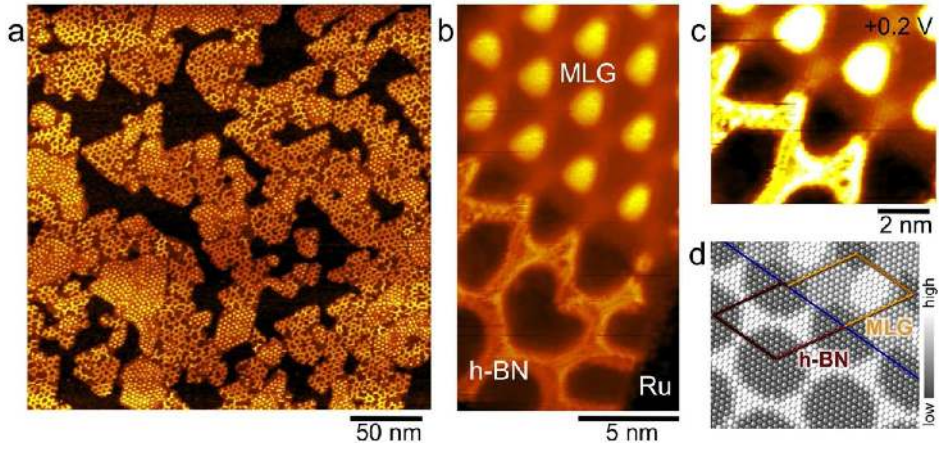

Figure 6. Graphene-boron nitride heterostructures with atomically sharp interfaces. (a) Overview STM image showing nanoscale graphene domains with attached h-BN. (b) High-resolution STM image of the interface between graphene (MLG) and boron nitride (h-BN) on Ru(0001). (c) Zoomed-in view of the interfacial boundary. (d) Schematic elevation map of MLG and h-BN moirés (unit cells outlined) joined in an abrupt zigzag boundary (blue line).

with a clearly resolved honeycomb lattice and occur isolated or bunched into larger groups with local ordering (Figure 4c). Their size is comparable to a single honeycomb unit (fwhm ~3 Å) and their appearance is similar to substitutional dopants in graphene.[22] Therefore, the STM observations are consistent with a substitutional B−C−N phase near the MLG/h-BN interface. Pairwise incorporation of C in nearest-neighbor B/N sites was found in atomic-scale holes in free-standing h-BN membranes,[33] and a similar mechanism may lead to C incorporation into the edges of supported h-BN. Indeed, AES composition profiles (Figure 2c) show similar widths of the transition region for C and (B, N), suggesting that C can substitute for both B and N in the growing h-BN film.

The population of C adatoms on the Ru surface in the presence of graphene at high temperatures (Supporting Information Figure S1)[28] provides an ample C supply for substitutional incorporation into h-BN. Reducing the BN growth temperature can lead to narrower interfacial B−C−N zones (as seen, for example, in Figure 3) but is not sufficient to realize graphene-boron nitride heterostructures with atomically sharp interfaces. To achieve this goal, processes need to be developed to eliminate C adatoms from the metal surface. The reaction of C/Ru(0001) with oxygen (O_2) to CO and desorption at high temperatures provides a possible avenue for eliminating C monomers, but it needs to be considered carefully since O_2 can also efficiently etch graphene.[34,35] Figure 5 shows real-time measurements of the C adatom concentration on Ru (as illustrated in Supporting Information Figure S1b−d) demonstrating the selective removal of C monomers by controlled O_2 exposure. Here, the growth of MLG domains on Ru (Figure 5a) by ethylene CVD at 750 °C is followed by exposure to low O_2 pressures at reduced temperature. During the entire process, both the C adatom concentration on the Ru surface and the size of the graphene domains are monitored (Figure 5b). The initial ethylene exposure rapidly builds up a population of C monomers. Graphene nucleation and growth draws from this C reservoir, but C adatoms remain on the Ru surface even after stopping the ethylene dose. Low-pressure O_2 exposure gradually lowers the C concentration while leaving the area of the MLG domains nearly unchanged. The graphene etch rate only increases after the C adatom density has saturated at a level equivalent to clean Ru. By controlling the

dx.doi.org/10.1021/nl302398m | Nano Lett. 2012, 12, 4869−4874

temperature and O_2 dose, graphene domains surrounded by Ru with very low C monomer concentration, comparable to carefully cleaned Ru(0001) without graphene, can be achieved (Supporting Information Figure S2). At higher temperatures, O_2 initially removes some C but the high equilibrium concentration of C adatoms is rapidly restored after terminating the O_2 dose (Supporting Information Figure S3).

We assessed the impact of C elimination by low-pressure O_2 exposure on the formation of MLG/h-BN boundaries by nano-AES, and at the atomic scale by cryogenic STM (Figure 6). AES line scans on samples prepared in three steps, MLG growth, O_2 etching of C adatoms, and h-BN growth, show abrupt composition changes across the MLG/h-BN interface (Supporting Information Figure S4). STM images (Figure 6) display a morphology that is strikingly different from that in Figures 3 and 4. While the preferential attachment of h-BN to MLG is maintained, interfacial regions without moiré structure are now completely absent, that is, the MLG and h-BN moirés join in a sharp boundary (Figure 6a). This is underscored by high-resolution imaging of a linear interface (Figures 6b–d), which shows an example of the atomic-scale bonding of the two materials in a zigzag boundary without any discernible intermediate structure.

Our results demonstrate that mixed B–N–C phases, consisting of h-BN doped with C, form spontaneously during sequential graphene and boron nitride growth on Ru. The primary mechanism for generation of these mixed phases is incorporation of C adatoms from the metal surface into the growing h-BN monolayer. Undoped h-BN forms only after this C reservoir is depleted. These results suggests that it should be possible to devise processes for the controlled synthesis of B–N–C "alloys" with tunable composition on transition metals and more generally to exploit the synthesis on metals to achieve nonequilibrium structures that are unstable (or metastable) in isolated 2D materials. By eliminating this C source, atomically sharp graphene-boron nitride interfaces are achieved. The realization of sharp linear interfaces between metal supported 2D materials opens up a rich field for studying the 1D equivalent of the more familiar 2D interfaces in thin film heterostructures, for example, effects of lattice mismatch, the formation and stability of polar and nonpolar interfaces, and so forth. Our work also shows a path toward the controlled synthesis of nanoscale graphene-boron nitride heterostructures. Processes similar to that demonstrated here can be applied to terminate the edges of nanographene, such as quantum dots[36] or atomically controlled ribbons[37] via their embedding in a monolayer h-BN membrane, thus providing avenues for facilitating the handling of wafer-scale arrays of graphene nanostructures by inserting them into insulating BN, and setting the stage for realizing the fascinating electronic properties predicted for graphene-boron nitride junctions in monolayer sheets.

Methods. We have used in situ microscopy to analyze the formation of single layer graphene-boron nitride heterostructures on Ru(0001) single crystals and epitaxial Ru(0001) thin films on sapphire substrates. Ru single crystal surfaces were prepared by the standard method, involving several cycles of oxygen adsorption and flashing to temperatures above 1400 °C. Epitaxial Ru films were grown by magnetron sputtering on *c*-axis oriented sapphire substrates, as described previously.[38] The growth of graphene and boron nitride was performed in UHV by exposure of the metal surface at high temperatures to high-purity ethylene and borazine, respectively. Additional processing involved the exposure of the samples to research grade (99.9999%) oxygen. Bright-field LEEM in an Elmitec LEEM V field-emission microscope was used to observe synthesis and processing in real time. Sample temperatures were measured using a W–Re thermocouple spot-welded onto the metal sample support. The structure of the different phases of heterogeneous graphene-boron nitride monolayers was characterized by selected-area low-energy electron diffraction (micro-LEED), as well as by room-temperature and low-temperature STM in separate UHV systems with in situ growth capability, with samples prepared using processes identical to those of our real-time LEEM investigation. Atomic-resolution imaging of the interfacial boundary between graphene and h-BN was performed in a low-temperature STM system (Createc) at a temperature of 78 K. UHV scanning electron microscopy (SEM) and chemical analysis by scanning Auger microscopy were performed using a field-emission SEM column (Gemini UHV) operated at 3 keV and a hemispherical electron energy analyzer (Omicron NanoSAM).

■ ASSOCIATED CONTENT

Supporting Information

Supplementary Figures S1–S4 and supplementary references. This material is available free of charge via the Internet at http://pubs.acs.org.

■ AUTHOR INFORMATION

Corresponding Author

*E-mail: psutter@bnl.gov.

Notes

The authors declare no competing financial interest.

■ ACKNOWLEDGMENTS

This research has been carried out at the Center for Functional Nanomaterials, Brookhaven National Laboratory, which is supported by the U.S. Department of Energy, Office of Basic Energy Sciences, under Contract No. DE-AC02-98CH10886.

■ REFERENCES

(1) He, J.; Chen, K.-Q.; Fan, Z.-Q.; Tang, L.-M.; Hu, W. P. *Appl. Phys. Lett.* **2010**, *97* (19), 193305.
(2) Li, J.; Shenoy, V. B. *Appl. Phys. Lett.* **2011**, *98* (1), 013105.
(3) Jun, S.; Li, X.; Meng, F.; Ciobanu, C. V. *Phys. Rev. B* **2011**, *83* (15), 153407.
(4) Ramasubramaniam, A.; Naveh, D. *Phys. Rev. B* **2011**, *84* (7), 075405.
(5) Jiang, J.-W.; Wang, J.-S.; Wang, B.-S. *Appl. Phys. Lett.* **2011**, *99* (4), 043109.
(6) Son, Y.-W.; Cohen, M. L.; Louie, S. G. *Nature* **2006**, *444* (7117), 347–349.
(7) Bhowmick, S.; Singh, A. K.; Yakobson, B. I. *J. Phys. Chem. C* **2011**, *115* (20), 9889–9893.
(8) Pruneda, J. M. *Phys. Rev. B* **2010**, *81* (16), 161409.
(9) Ohtomo, A.; Hwang, H. Y. *Nature* **2004**, *427* (6973), 423–426.
(10) Reyren, N.; Thiel, S.; Caviglia, A. D.; Kourkoutis, L. F.; Hammerl, G.; Richter, C.; Schneider, C. W.; Kopp, T.; Rüetschi, A.-S.; Jaccard, D.; Gabay, M.; Muller, D. A.; Triscone, J.-M.; Mannhart, J. *Science* **2007**, *317* (5842), 1196–1199.
(11) Oshima, C.; Nagashima, A. *J. Phys: Condens. Matter* **1997**, *9* (1), 1.
(12) Sutter, P. W.; Flege, J.-I.; Sutter, E. A. *Nat. Mater.* **2008**, *7* (5), 406–411.
(13) Reina, A.; Jia, X.; Ho, J.; Nezich, D.; Son, H.; Bulovic, V.; Dresselhaus, M. S.; Kong, J. *Nano Lett.* **2009**, *9*, 30–35.

(14) Li, X.; Cai, W.; An, J.; Kim, S.; Nah, J.; Yang, D.; Piner, R.; Velamakanni, A.; Jung, I.; Tutuc, E.; Banerjee, S. K.; Colombo, L.; Ruoff, R. S. *Science* **2009**, *324* (5932), 1312−1314.
(15) Corso, M.; Auwarter, W.; Muntwiler, M.; Tamai, A.; Greber, T.; Osterwalder, J. *Science* **2004**, *303* (5655), 217−220.
(16) Sutter, P.; Lahiri, J.; Albrecht, P.; Sutter, E. *ACS Nano* **2011**, *5* (9), 7303−7309.
(17) Kim, K. K.; Hsu, A.; Jia, X.; Kim, S. M.; Shi, Y.; Hofmann, M.; Nezich, D.; Rodriguez-Nieva, J. F.; Dresselhaus, M.; Palacios, T.; Kong, J. *Nano Lett.* **2011**, *12*, 161−166.
(18) Liu, Z.; Song, L.; Zhao, S.; Huang, J.; Ma, L.; Zhang, J.; Lou, J.; Ajayan, P. M. *Nano Lett.* **2011**, *11* (5), 2032−2037.
(19) Ci, L.; Song, L.; Jin, C.; Jariwala, D.; Wu, D.; Li, Y.; Srivastava, A.; Wang, Z. F.; Storr, K.; Balicas, L.; Liu, F.; Ajayan, P. M. *Nat. Mater.* **2010**, *9* (5), 430−435.
(20) Zhu, J.; Bhandary, S.; Sanyal, B.; Ottosson, H. *J. Phys. Chem. C* **2011**, *115* (20), 10264−10271.
(21) Endo, M.; Hayashi, T.; Hong, S.-H.; Enoki, T.; Dresselhaus, M. S. *J. Appl. Phys.* **2001**, *90* (11), 5670−5674.
(22) Zhao, L.; He, R.; Rim, K. T.; Schiros, T.; Kim, K. S.; Zhou, H.; Gutiérrez, C.; Chockalingam, S. P.; Arguello, C. J.; Pálová, L.; Nordlund, D.; Hybertsen, M. S.; Reichman, D. R.; Heinz, T. F.; Kim, P.; Pinczuk, A.; Flynn, G. W.; Pasupathy, A. N. *Science* **2011**, *333* (6045), 999−1003.
(23) Martoccia, D.; Willmott, P. R.; Brugger, T.; Bjorck, M.; Gunther, S.; Schleputz, C. M.; Cervellino, A.; Pauli, S. A.; Patterson, B. D.; Marchini, S.; Wintterlin, J.; Moritz, W.; Greber, T. *Phys. Rev. Lett.* **2008**, *101* (12), 126102−4.
(24) Goriachko, A.; He; Knapp, M.; Over, H.; Corso, M.; Brugger, T.; Berner, S.; Osterwalder, J.; Greber, T. *Langmuir* **2007**, *23* (6), 2928−2931.
(25) Longo, R. C.; Stepanyuk, V. S.; Hergert, W.; Vega, A.; Gallego, L. J.; Kirschner, J. *Phys. Rev. B* **2004**, *69* (7), 073406.
(26) Sutter, P.; Schwarz, C.; Muller, E.; Zelezny, V.; Goncalves-Conto, S.; von Kanel, H. *Appl. Phys. Lett.* **1994**, *65* (17), 2220−2222.
(27) Tersoff, J. *Phys. Rev. Lett.* **1995**, *74*, 434−437.
(28) Loginova, E.; Bartelt, N. C.; Feibelman, P. J.; McCarty, K. F. *New J. Phys.* **2008**, *10*, 093026.
(29) Sutter, P.; Ciobanu, C. V.; Sutter, E. *Small* **2012**, *8* (14), 2250−2257.
(30) Wang, B.; Bocquet, M.-L.; Marchini, S.; Günther, S.; Wintterlin, J. *Phys. Chem. Chem. Phys.* **2008**, *10*, 3530−3534.
(31) Sutter, E. A.; Acharya, D. P.; Sadowski, J. T.; Sutter, P. W. *Appl. Phys. Lett.* **2009**, *94*, 133101.
(32) Laskowski, R.; Blaha, P.; Gallauner, T.; Schwarz, K. *Phys. Rev. Lett.* **2007**, *98*, 106802.
(33) Krivanek, O. L.; Chisholm, M. F.; Nicolosi, V.; Pennycook, T. J.; Corbin, G. J.; Dellby, N.; Murfitt, M. F.; Own, C. S.; Szilagyi, Z. S.; Oxley, M. P.; Pantelides, S. T.; Pennycook, S. J. *Nature* **2010**, *464* (7288), 571−574.
(34) Sutter, P.; Sadowski, J. T.; Sutter, E. A. *J. Am. Chem. Soc.* **2010**, *132* (23), 8175−8179.
(35) Cui, Y.; Fu, Q.; Zhang, H.; Tan, D.; Bao, X. *J. Phys. Chem. C* **2009**, *113* (47), 20365−20370.
(36) Lu, J.; Yeo, P. S. E.; Gan, C. K.; Wu, P.; Loh, K. P. *Nat. Nanotechnol.* **2011**, *6* (4), 247−252.
(37) Cai, J.; Ruffieux, P.; Jaafar, R.; Bieri, M.; Braun, T.; Blankenburg, S.; Muoth, M.; Seitsonen, A. P.; Saleh, M.; Feng, X.; Mullen, K.; Fasel, R. *Nature* **2010**, *466* (7305), 470−473.
(38) Sutter, P. W.; Albrecht, P. M.; Sutter, E. A. *Appl. Phys. Lett.* **2010**, *97* (21), 213101.

Supplementary Online Material

Interface Formation in Monolayer Graphene-Boron Nitride Heterostructures

P. Sutter, R. Cortes, J. Lahiri, and E. Sutter
Center for Functional Nanomaterials, Brookhaven National Laboratory, Upton, New York 11973, USA

Supplementary Figures

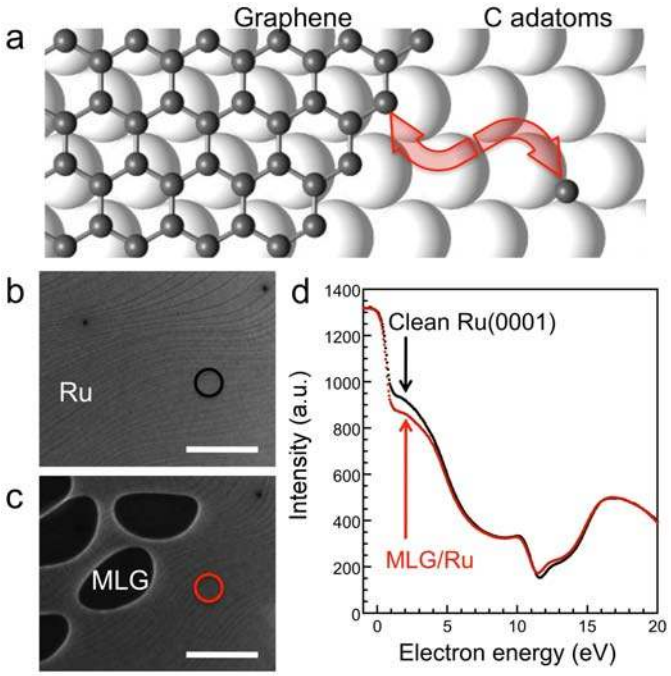

Figure S1 – Thermal C adatoms in equilibrium with graphene on Ru(0001). (a) Schematic representation of a graphene domain on Ru(0001), in equilibrium with C monomers bound in threefold hollow sites of the Ru surface mesh. The strong binding of C atoms on Ru(0001) causes a sizable C monomer population on Ru(0001) in equilibrium with graphene at high temperatures.[1] **(b), (c)** LEEM images of clean Ru(0001), and of the surface following the nucleation of monolayer graphene domains (MLG). **(d)** LEEM I-V spectra obtained at T = 700°C on clean Ru(0001) [black circle in (b)] and on the Ru surface adjacent to graphene domains [red circle in (c)] show a characteristic reduction of the reflected intensity near V ≈ 2 eV. The intensity reduction is proportional to the coverage of C monomers on the Ru surface, i.e., can be used to track the monomer concentration during further processing designed to eliminate C monomers from the surface.

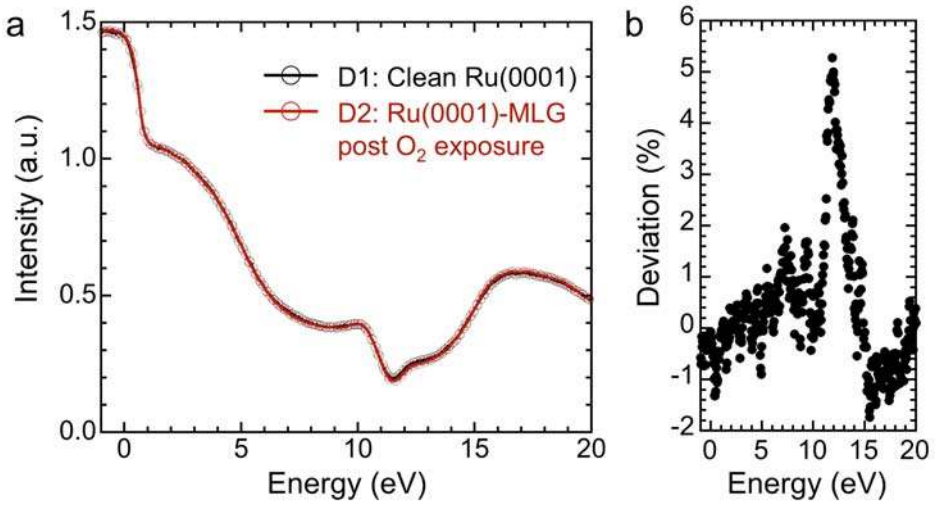

Figure S2 – Comparison of meticulously cleaned Ru(0001) with Ru(0001) carrying graphene domains, following the O_2 induced removal of C monomers. **(a)** LEEM I-V curves for a clean Ru(0001) surface without graphene, obtained by the standard procedure (cycles of O_2 adsorption/flashing to > 1400°C); and for a Ru(0001) surface with partial graphene coverage, for which C monomers on the metal have been selectively removed by O_2 exposure (2×10^{-9} Torr, 610°C), following a procedure identical to that used in fig. 4. The two I-V curves were measured under identical conditions. For the comparison, the data were normalized to the same intensity at the lowest electron energy, E = -1 eV. Symbols represent a subset (every 3rd point) of the experimental data. **(b)** Deviation between the two data sets D1 and D2 shown in fig. S2a, expressed as (D1 – D2)/D1 (in percent). The difference between the I-V characteristics is smaller than ±1.5% for all electron energies except near the minimum at E ~ 12 eV. In particular, the difference at E ~ 2 eV, which is proportional to the density of C adatoms, is < 1%. Hence, the data sets D1 and D2 are virtually indistinguishable, demonstrating the efficient C removal from the metal surface by low-pressure O_2 exposure, despite the presence of graphene domains.

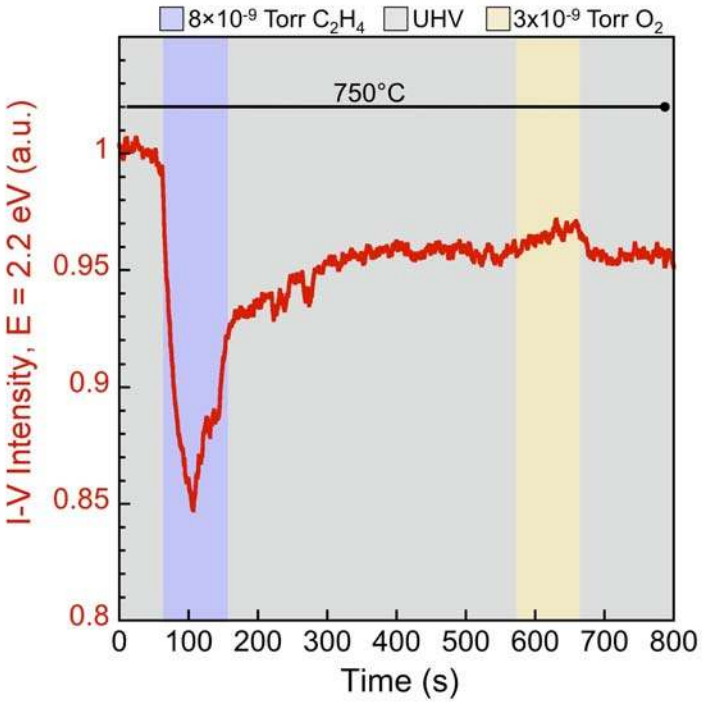

Figure S3 – Oxygen-induced removal of thermal C adatoms on Ru(0001) at 750°C. Time-dependent LEEM I-V intensity at 2.2 eV electron energy during graphene growth and O_2 exposure at 750°C. Low-pressure O_2 exposure of the Ru surface with partial graphene coverage leads to removal of some C from the surface (increase in intensity between ~575 s – 665 s), but the higher equilibrium C concentration is rapidly restored upon termination of the O_2 dose.

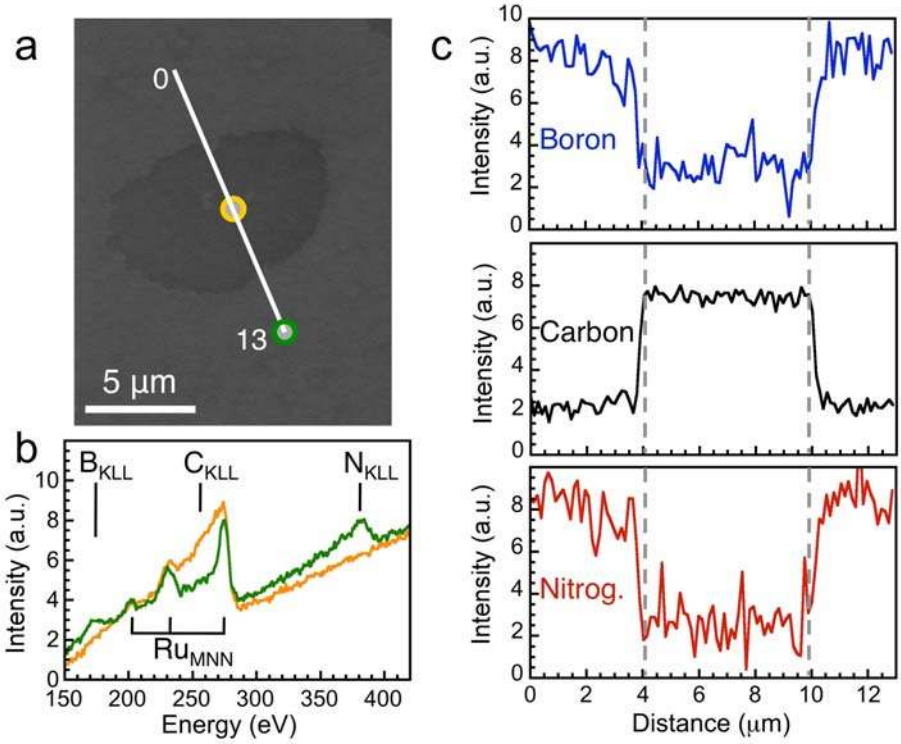

Figure S4 – Nano-Auger spectroscopy analysis of a monolayer graphene-boron nitride heterostructure grown by sequential graphene CVD (ethylene, 10^{-8} Torr, 780°C), oxygen etching of C adatoms (O_2 2 × 10^{-9} Torr, 680°C), and h-BN growth (borazine, 10^{-8} Torr, 680°C). (a) UHV SEM image of a MLG domain embedded in a continuous h-BN layer. **(b)** Auger electron spectra at points near the center of the MLG domain and in the h-BN layer, marked in (a). **(c)** Nano-AES line scans for B_{KLL} (171.6 eV), C_{KLL} (260.6 eV), and N_{KLL} (380.0 eV) Auger lines, along the line marked in (a).

References

1. Loginova, E.; Bartelt, N. C.; Feibelman, P. J.; McCarty, K. F. *New Journal of Physics* **2008,** 10, 093026.